A method for quantifying, visualising, and analysing gastropod shell form

Quantitative analysis of organismal form is an important component for almost every branch of biology. Although generally considered an easily-measurable structure, the quantification of gastropod shell form is still a challenge because shells lack homologous structures and have a spiral form that is difficult to capture with linear measurements. In view of this, we adopt the idea of theoretical modelling of shell form, in which the shell form is the product of aperture ontogeny profiles in terms of aperture growth trajectory that is quantified as curvature and torsion, and of aperture form that is represented by size and shape. We develop a workflow for the analysis of shell forms based on the aperture ontogeny profile, starting from the procedure of data preparation (retopologising the shell model), via data acquisition (calculation of aperture growth trajectory, aperture form and ontogeny axis), and data presentation (qualitative comparison between shell forms) and ending with data analysis (quantitative comparison between shell forms). We evaluate our methods on representative shells of the genus *Opisthostoma*, which exhibit great variability in shell form. The outcome suggests that our method is more robust, reproducible, and versatile than the conventional traditional and geometric morphometric approaches for the analysis of shell form. Finally, we propose several potential applications of our methods in functional morphology, theoretical modelling, taxonomy, and evolutionary biology.

PeerJ PrePrints | https://peerj.com/preprints/157v1/ | v1 received: 16 Dec 2013, published: 16 Dec 2013, doi: 10.7287/peerj.preprints.157v1

Thor-Seng Liew and Menno Schilthuizen

1 Institute Biology Leiden, Leiden University, P.O. Box 9516, 2300 RA Leiden, The Netherlands.

2 Naturalis Biodiversity Center, P.O. Box 9517, 2300 RA Leiden, The Netherlands.

3 Institute for Tropical Biology and Conservation, Universiti Malaysia Sabah, Jalan UMS, 88400, Kota Kinabalu, Sabah, Malaysia.

Email: T-S L: thorsengliew@gmail.com

MS: Menno.Schilthuizen@naturalis.nl

Funding: This study is funded under project 819.01.012 of Research Council for Earth and Life Sciences (ALW-NOW). The funders had no role in study design, data collection and analysis, decision to publish, or preparation of the manuscript.

Competing interests: The authors have declared that no competing interests exist.

Introduction

Empirical and theoretical approach in the study of shell form

The external form diversity of organisms is the most obvious evidence for their evolution, and thus is a key element in most branches of biology. The Molluscan shell has been a popular example in morphological evolution studies because it is geometrically simple, yet diverse in form. The shell form is controlled by the shell ontogenetic process, which follows a simple accretionary growth mode where new shell material is accumulatively deposited to the existing aperture. The evolution of shell forms has been studied either by using empirical approaches that focus on the quantification of actual shell forms or by using theoretical approaches that focus on the simulation of shell ontogenetic processes and geometric forms.

Notwithstanding the active development in both empirical and theoretical approaches to the study of shell form, there has been very little integration between both schools. For the empirical approach, the quantification methods of shell form have evolved from traditional linear measurement to landmark-based geometric morphometrics and outline analyses (for an overview see Van Bocxlaer & Schultheiß, 2010). At the same time, for the theoretical approach, the simulations of shell form have evolved from simple geometry models that aimed to reproduce the form, to more comprehensive models that simulate shell ontogenetic processes (for an overview see Urdy et al., 2010). Hence, each of the two approaches has been moving forward but away from each other, where synthesis between the two schools of shell morphologists has become more challenging.

In empirical morphological studies, shell form, either in terms of heights and widths in traditional morphometrics or in terms of geometry of procrustes distances in geometric morphometrics, is quantified by a set of homologous reference points or landmarks on the shell, which can be easily obtained from the fixed dimensions of the shell. Thus, both methods could abstract the shell form in terms of size and shape of the particular shell dimensions, and the between-sample variation of shell size and shape can be assessed (in most cases only within one study). On the other hand, it is not possible to reconstruct the actual shell form from these quantitative measurements, because the shell's accretionary growth model and spiral geometry cannot be quantified on the basis of arbitrary reference points or fixed dimensions (Stone. 1997). Nevertheless, the traditional and geometric morphometric methods have been accepted widely as standard quantification methods for shell form in many different fields of research.

In contrast to empirical morphometrics in which the aim is to quantify the actual shell, theoretical morphologists focus on the simulation of an accretionary growth process which produces a shell form that is similar to actual shells. This field was established with the theoretical shell model of D.M. Raup (Raup, 1961; Raup & Michelson, 1965). Within the first two decades after these publications, only a few different versions of shell models were proposed (e.g. Løvtrup & von Sydow, 1974; Bayer, 1978; McGhee, 1978; Kawaguchi, 1982; Illert, 1983). The subsequent two decades, thanks to the popularity and power of desktop computing, many more theoretical shell models were published (e.g., Savazzi, 1985; Okamoto, 1988; Cortie, 1989; Ackerly, 1989a; Savazzi, 1990; Checa, 1991; Fowler et al., 1992; Illert & Pickover, 1992; Checa & Aguado, 1992; Cortie, 1993; Savazzi, 1993; Rice, 1998; Ubukata, 2001; Galbraith, Prusinkiewicz & Wyvill, 2002). Finally, we saw further improvements in the published theoretical models in recent years. These recent models simulate shell forms that more accurately resemble actual shells because of improved programming software, better algorithms, and 3D technology (e.g. Picado, 2009, Stępień, 2009; Meinhardt, 2009; Urdy et al., 2010; Harary & Tal, 2011; Moulton & Goriely, 2012; Moulton, Goriely & Chirat, 2012; Faghih Shojaei et al., 2012; Chacon, 2012). Here, we will not further discuss the details of the at least 29 published shell models, but refer to the comprehensive overviews and descriptions of these models in Dera et al. (2009) and Urdy et al. (2010).

In brief, the latest theoretical shell models are able to simulate irregularly-coiled shell forms and ornamentations that resemble actual shells, whereas the earlier models could only simulate the regular and general shape of shells. The major refinements that have been made during the almost five decades' development of theoretical shell models are the following modifications of the algorithm: 1) from a fixed reference frame to a moving reference frame system; 2) from modelling based on numerical geometry parameters to growth-parameter-based modelling (e.g. growth rates); 3) from three parameters to more than three parameters, which has made fine-tuning of the shell simulation (e.g. aperture shape) possible. The key element of the theoretical modelling of shells is the generation of shell form by simulating the aperture ontogeny in terms of growth trajectory and form along the shell ontogeny. Hence, this has an advantage over the empirical approach in the numerical representation of the shell geometry form in terms of the 3D quantification and the actual shell ontogenetic processes.

Since the empirical and theoretical researchers studying shell form with two totally different quantification methods, our understanding of shell evolution cannot progress solely by using either empirical morphometrics or theoretical models. Ideally, theoretical models need to be evaluated by empirical data of shell morphometrics, and, vice-versa, empirical morphometric methods need to be improved to obtain data that better reflect the actual shell form and morphogenesis which can then be used to improve the theoretical models. In this dilemma lies the central problem of shell form quantification and it urgently needs to be addressed in order to integrate and generalise studies of shell form evolution.

Why empirical morphologists rarely use theoretical shell models

Despite the fact that, since the 1980s, manyshell models have been published that are more complex and versatile, the first theoretical shell model of Raup still remains the most popular. There were many attempts by empirical morphologists to use the original or a modified version of Raup's parameters to quantify natural shell forms (e.g. Raup, 1967; Vermeij, 1971; Davoli & Rosso, 1974; Graus, 1974; Kohn & Riggs, 1975; Newkirk & Doyle, 1975; Warburton, 1979; Verduin, 1982; Ekaratne & Crisp, 1983; Saunders & Shapiro, 1986; Tissot, 1988; Foote & Cowie, 1988; Johnston, Tabachnick & Bookstein, 1991; Emberton, 1994; Clarke, Grahame & Mill, 1999; Samadi, David & Jarne, 2000). Surprisingly, all the other shell models, many of which produce more realistic forms, have received very little attention as compared to Raup's model (see e.g. Savazzi, 1992; Okajima & Chiba, 2011; Okajima & Chiba, 2012, for exceptions). This ironic situation might be explained by the elegance of Raup's model that is intuitively and mathematically simple to be used by empirical morphologists (mostly biologists), with limited mathematical and programming experience.

As discussed above, most of the theoretical models can simulate a shell that has a form resembling the actual shell in a realistic 3D geometry, based on shell ontogeny processes. In contrast, empirical morphometrics can only quantify and compare certain dimensions of actual shells. Clearly, the theoretical approach is better than the empirical approach in its accuracy of shell form quantification, because accurate morphological quantification is essential for functional, ecological and evolutionary studies of shell form. Below, we identify and discuss a few impediments that currently prevent empirical morphologists from adopting the theoretical approach in shell form quantification.

First, the requirement of a computation resource was an impediment in the past. These theoretical models may only be implemented in a computation environment. As mentioned above, the advances of computation hardware in speed and 3D graphic technology have promoted the development of more complex theoretical shell models. For example, the current speed and storage of a desktop computer is at least four orders of magnitude greater than those used by Cortie (1993) only two decades ago. Clearly, the computation hardware is no longer an impediment (e.g. Savazzi, 1995) for the application and development of theoretical shell models.

Notwithstanding the hardware development, programming skills are still a prerequisite for the implementation of theoretical models. Many of the early models that were published between the 1960s and 1990s, used third-generation programming languages such as Fortran and C++, which essentially lack a graphic user interface. This situation has improved now that the simulation of theoretical shell models can be done in fourth-generation programming languages such as Mathematica (e.g. Meinhardt, 2009; Noshita, 2010; Okajima & Chiba, 2011; Okajima & Chiba, 2012) and MATLAB (e.g. Boettiger, Ermentrout & Oster, 2009; Urdy et al. 2010, Faghih Shojaei et al., 2012). Most of these shell models were described with intensive mathematical notation, at least from a biologist's point of view, in the publication; and some of these were published together with the information on algorithm implementation. However, the actual programming codes are rarely published together with the paper though they may be available from the authors upon request (but see Meinhardt, 2009; Noshita, 2010; Okajima & Chiba, 2011). Only one theoretical modelling software package based on Raup's model has a graphic user interface that is comparable to contemporary geometric morphometric software (Noshita, 2010). Thus, the rest of the modern theoretical models are far less approachable than the morphometric software for empirical morphologists. This is because those advanced theoretical models have not been delivered in a form that allowed empirical morphologists to have "hands-on experience" with them, without extensive mathematical literacy (Savazzi, 1995; McGhee, 2007).

Second, theoretical shell models simulate the shell form based on the input of a set of parameters, which could be non-biological or/and biologically meaningful. Non-biological meaningful parameters are counter-intuitive for empirical morphologists because these parameters are not extrinsic shell traits. Nevertheless, many of these non-biological parameters are required for the model to fit the shell form schematically (Hutchinson, 1999). When the biological parameters do

represent shell traits, they are often difficult to obtain accurately and directly from the actual shell because of the three-dimensional spiral geometry (Cain, 1977; Ackerly, 1989a; Ackerly, 1989b; Okamoto, 1988; Schindel, 1990; Checa & Aguado, 1992, Hutchinson, 1999; McGhee, 1999). Since the development of theoretical shell models, almost all simulated shell models have been made by an ad hoc approach, where the parameters are chosen for the model and then the simulated shells are compared with the actual shells. In almost all cases, the correct parameters are chosen after a series of trial-and-error, and the parameters are selected when the form of the simulated shell matches the actual shell. Okamoto (1988) suggested that this ad hoc approach based on pattern matching was easier than obtaining the parameters empirically from the shell.

Third, although the overall forms of the simulated shells resemble the actual shells, the simulated shell is not exactly the same as the actual shell (Kohn & Riggs, 1975; Goodfriend, 1983). For many models, its original parameters are not sufficient to simulate the shell form exactly (Schindel, 1990; Fowler, Meinhardt & Prusinkiewicz, 1992). These simulated general shell forms are adequate for theoretical morphologist interests in their exploration of general shell forms. However, the subtle features on a real shell or the subtle differences among different shell forms of real species that cannot be simulated by theoretical models may have significant functional implications that are important for empirical morphologists.

In brief, it is clear that the implementation of current theoretical shell models is less accessible to empirical shell morphologists. Yet, empirical morphologists are using traditional and geometric morphometrics as a routine method for shell quantification.

Why empirical morphologists use traditional and geometric morphometrics

In addition to the impediments arising from the theoretical shell model itself that are limiting its popularity among empirical morphologists, the theoretical approach faces competition from geometric morphometric methodology. The popularisation of desktop computing that led to the flourishing of theoretical shell models in the late 1980s, also promoted the development of morphometric methods, such as Elliptical Fourier Analysis (EFA) and geometric morphometrics (GM). Rohlf and Archie (1984) set a benchmark for the quantification of an organism's form by EFA, which was improved from Kaesler and Waters (1972) and Kuhl and Giardina (1982). Rohlf and Slice (1990) and Bookstein (1991) developed a complete standard protocol for GM. Soon

after these pioneer papers, various software with Graphic User Interface (GUI) were developed for the application of EFA and GM (Cardini & Loy, 2013, see http://life.bio.sunysb.edu/morph/). In contrast to the application of theoretical shell models, an understanding of mathematics and programming languages is not a prerequisite for the user of these morphometric tools. Thus, EFA and GM have been well received by biologists, and have been adopted in the morphometric study of shell form.

These geometric morphometric software packages have standard and interactive workflows that help empirical morphologists in every step of: obtaining morphometric data (e.g. placing landmark coordinates), analysing data (e.g. procrustes superimposition), statistical analysis (e.g. ANOVA, PCA), and visualising shape and shape changes (e.g. thin-plate spline, PCA plots). This has made geometric morphometrics approachable and attractive to empirical morphologists, who want to examine the similarities and differences among shell forms.

Geometric morphometrics is actually a statistic of shape that is calculated from Cartesian coordinate data from a sample of objects (Cardini & Loy, 2013). However, it is not an exact quantification of form and is not particularly suitable for comparison and quantification of shell form, for the following two reasons.

First, GM analysis is based on homologous landmarks on the form, but shell has only arbitrary landmarks because it has a low degree of morphological complexity (Van Bocxlaer & Schultheiß 2010). In most cases, 2D landmarks are chosen at the shell apex, suture, and aperture or whorl outline that can be identified from a 2D image that is taken in standard apertural view of a shell. These landmarks are chosen to be analysed by GM but these points have little biological meaning. Furthermore, as opposed to the form of many other organisms, 3D landmarks are even more difficult to be obtained from a shell (3D model) as compared to 2D landmarks because many of these landmarks, such as suture points, that are obtained from a 2D image are just artefacts of the fixed 2D view of the shell.

Second, the results of separate, independent studies of shell forms cannot be integrated, even though these studies use the same GM method. Statistical analysis of the Cartesian coordinate data that abstractly represent the shell form is adequate in quantifying the variation of a shell within a context of other shells that are included in a single study or within similar taxa where

similar landmarks are obtained. However, the raw coordinate data and analysed shape variation from a study are incomparable and incompatible with the data from other studies (Klingenberg, 2013).

Despite the fact that geometric morphometrics has been widely used by empirical morphologists, it is not an ideal tool in the quantification of shell form for the reasons given above. The increasing availability of the software and application in the literature might cause morphologists to stray away from their initial aims of studying shell form. Hence, it is important to return to the core of the question: what do biologists want to learn from the study of shell form? Clearly, in addition to quantitatively compare shell forms, biologists want to know more about the general characteristics and physical properties of the shell form that are key elements in gaining insight into functional and ecological aspects of the shell (Evans, 2013). However, functional and ecological aspects of shell form can only be determined if the shell form can be exactly quantified.

Using 3D technology to quantify shell form based on aperture ontogeny profiles

In this paper, we propose an interactive approach to the quantification and analysis of shell forms based on state of the art 3D technology and by integrating the theoretical principles of shell modelling and the empirical principles of morphometric data handling. There are no theoretical models that can simulate all existing shell forms. However, the theoretical background of the theoretical models is biologically sound – simulating the shell form by simulating the shell ontogenetic process. On the basis of this shell-ontogenesis principle, we used state-of-the-art X-ray microtomography (micro-CT scan) and 3D modelling software to obtain a series of shell aperture changes from the shell in an interactive workflow that is similar to empirical morphometric analysis.

First, a series of shell aperture outlines were digitised directly from the reconstructed 3D shell model obtained from micro-CT scanning by using open-source 3D-modelling software – Blender ver. 2.63 (www.blender.org). Then, the growth trajectory and form of the shell aperture outline were quantified and extracted with our custom scripts that run in Blender through its embedded open-source Python interpreter (http://www.python.org/). The changes of aperture size and shape, and aperture growth trajectory in terms of curvature and torsion along the shell ontogeny axis

length were obtained (hereafter "aperture ontogeny profiles"). The final aperture ontogeny profiles are in a form of multivariate time series data, which consist of a number of instances (i.e. number of quantified apertures that depends on the length of the whorled shell tube) and attributes that represent the growth trajectories, aperture form, and size.

These aperture ontogeny profiles can be plotted when each shell is examined individually. On the other hand, the aperture ontogeny profiles can be visually compared between different shells by plotting the data as radar chart (i.e. spider and star plots). In addition, the differences between shells can be assessed quantitatively by calculating the dissimilarity of aperture ontogeny profiles among shells. Furthermore, the dissimilarity matrix can be used to plot the dendrogram and NMDS plots, which resemble a shell morphospace. All our procedures were implemented by using open source and free software.

Finally, we discuss some possible applications and implications of these shell form quantification methods in theoretical morphology, functional morphology, taxonomy and shell shape evolutionary studies.

Materials and Methods

Ethics Statement

Specimens were collected in Malaysia with permissions from the Economic Planning Unit, Malaysia (UPE: 40/200/19/2524).

Scanning instrumentation

A micro-CT scanner (SkyScan, model 1172, Aartselaar, Belgium) and its accompanying software, NRecon ver. 1.6.6.0 (Skyscan©) and CT Analyser ver. 1.12.0.0 (Skyscan©), were used to generate digital shell 3D models from the actual shell specimens.

Computation software and hardware

Various commercial 3D modelling and statistical software exist for visualising, manipulating, and understanding morphology, such as Amira® (Visage Imaging Inc., San Diego, CA) and Autodesk Maya (San Rafael, CA) (reviewed by Abel, Laurini & Richter, 2012). However, in this study, we used only two open-source 3D data modelling and processing software packages, namely Blender

ver. 2.63 (www.blender.org) and Meshlab ver. 1.3.2 (Cignoni, Corsini & Ranzuglia, 2008, http://meshlab.sourceforge.net/). Both have been used in biology to visualise and model morphology (for Meshlab: Im et al., 2012; Chaplin, Yu & Ros, 2013; Atwood & Sumrall, 2012; for Blender: Pyka et al., 2010: 22); Haug, Maas & Waloszek, 2009; Cassola et al., 2010; Haug et al., 2010; Andrei et al., 2012; Haug et al., 2012; Lv et al., 2013; Mayer et al., 2012). However, these programs have not been used to their full extent in morphological quantification and analysis of 3D data for organisms. For quantification of morphology, we used the open-source Python interpreter ver. 3.2 that is embedded in Blender 2.63. In addition, we also used an extension to the Python programming language – NumPy (Oliphant, 2007) which consists of high-level mathematical functions.

All the morphological data were explored and analysed with the statistical open source programming language R version 3.0.1 (R Core Team, 2013) in the environment of RStudio (RStudio, 2012). We installed three additional packages in R, namely, "lattice": Lattice Graphics (Sarkar, 2008), "pdc": Permutation Distribution Clustering (Brandmaier, 2012a; Brandmaier, 2012b), and "fmsb" (Nakazawa, 2010).

All the computation analyses were carried out with a regular laptop computer with the following specifications: Intel®Core™i7-3612QM @ 2.1GHz, 8 GB memory (RAM), NVIDIA® GeForce GT 630M with 2GB memory.

Procedures

1. Obtaining digital 3D models from actual shells

The scan conditions were as follows: voltage – 80kV or 100kV; pixel – 1336 rows × 2000 columns; camera binning – 2 × 2; image pixel size – 3–6 µm; rotation step – 0.4° or 0.5°; and rotation – 360°. Next, the volume reconstruction on the acquired images was done in NRecon. The images were aligned to the reference scan and reconstruction was done on the following settings: beam hardening correction – 100%; reconstruction angular range – 360 degree; minimum and maximum for CS to image conversion (dynamic range) – ca. 0.12 and ca. 20.0; and result file type – BMP. Finally, 3D models were created from the reconstruction images in CT Analyser with the following setting: binary image index – 1 to 255 or 70 to 255; and were saved as digital polygon mesh object (*.PLY format).

2. Pre-processing digital shell models

The 3D models were then simplified by quadric edge collapse decimation implemented in MeshLab (Cignoni, Corsini & Ranzuglia, 2008) to reduce computation requirements. The raw polygon mesh shells in PLY format have millions of faces and a file size between 20 to 80 Mbytes. Thus, we reduced the number of faces for all model to 200,000 – 300,000 faces, which range between 3 and 6 Mbytes in file size. In addition, for the sake of convenience during the retopology processes, all 3D models were repositioned so that the shell protoconch columella was parallel with the z-axis. This was done by using manipulator tools in MeshLab.

3. Creating reference: Tracing aperture outlines and ontogeny axis from shell models

The digital shell 3D model in PLY format consists of 3D Cartesian coordinate vertices in which each of the three vertices constitutes a triangular face, and all faces are connected through a complex network. In order words, these vertices and faces are not biologically meaningful structures, and it is not possible to extract aperture outlines data directly from a raw PLY digital shell model. Monnet et al. (2009), for example, attempted to extract aperture outline automatically from a digital 3D model by making a plane cross-sectioning of the shell model, but its outlines do not reflect the form of the actual aperture outlines. Hence, we retopologised the raw 3D mesh models according to the aperture ontogeny for later data extraction.

We used Blender, which is more flexible than the commercial software used by Monnet et al. (2009). For the sake of convenience, we describe the following workflow, including the tools or the function (e.g. “Import PLY”) which can be called after hitting the SPACE bar while in the Blender environment. However, this workflow may be modified by the user.

To begin, we imported a PLY shell model into the Blender environment (“Import PLY”). Then, we resized the model 1000 × (“Resize”) so that the scale of 1 Blender unit was equal to 1 mm. After that, we examined the traces of aperture outlines (i.e. growth lines, ribs, spines) (Figure 1A) and ontogeny axis (i.e. spiral striation, ridges, colour lines) (Figure 1B) of the actual shells. After these aperture traits were identified, we selected the 3D model (by clicking “right mouse button”), and traced all these traits on the surface of the raw 3D mesh model in Blender by using the “Grease Pen Draw” tool. After that, the grease pen traced aperture traits were converted to Bezier curves with “Convert Grease Pencil” (Figure 1C).

4. Retopologising aperture outlines from the reference and generating retopologised shell models

For each shell, we created a set of new Non Uniform Rational B-Splines (NURBS) surface circles ("Add Surface Circle") and modified these ("Toggle Editmode") according to the aperture outlines. We created a 16 points NURBS surface circle and aligned the circle to the aperture outline by translation ("Translate"), rotation ("Rotate"), and resizing ("Resize") (Figure 1D). After the NURBS surface circle was generally aligned, each of the 16 points of the NURBS surface circle were selected and adjusted by translation ("G") one by one, so that the outline of the NURBS surface circle was exactly the same as the aperture outline. At the same time, the second point of the NURBS surface circle was aligned to the ontogeny axis (Figures 1B and 1C).

After the first aperture outline was retopologised as a NURBS surface circle, the NURBS surface circle was duplicated ("Duplicate Objects") and aligned to the next aperture outline as the previous one. This step was repeated until all the aperture outlines were retopologised into NURBS surface circles (Figures 1D and 1E). Then the shell surface was created in the form of a NURBS surface based on the digitised aperture NURBS surface circle ("(De)select All" and "Make Segment" in "Toggle Editmode") (Figures 1F and 1G). Lastly, we made the surface meet the end points in U direction and increased the surface subdivision per segment (resolution U = 8) through the properties menu of the object (Properties (Editor types)>Object Data>Active Spline).

After that, we converted the NURBS surface 3D model into a 3D Mesh model that consists of vertices, edges, and faces ("Convert to" - "Mesh from Curve/Meta/Surf/Text"). The final retopologised 3D shell Mesh consists of X number of apertures outlines and each aperture outline has Y number of vertices and then a total of X*Y vertices. Each of the vertices is connected to four other nearest vertices with edges to form a wireframe shell and face (Figure 1H).

It is important to note that the NURBS surface circle is defined by a mathematic formula which does not imply any biology perspective of the shell. We choose NURBS surface circle because the 3D aperture outline form can be digitalised by a small number of control points and shell surface can be recreated by NURBS surface based on the digitised aperture NURBS surface circle. The final 3D polygon mesh model is more simplified than the raw PLY 3D model and each of its vertex data resemble the actual accretionary process of the shell (Figures 1A and 1H).

5. Quantifying aperture growth trajectory

The aperture ontogeny profiles were quantified as described in Liew et al. (in press, b) with slight modifications where both aperture growth trajectory and aperture form were quantified directly from the retopologised 3D shell model. This aperture growth trajectory was quantified as a spatial curve, which is the ontogeny axis as represented by a series of first points of the aperture outlines. We estimated two differential geometry parameters, namely, curvature (κ) torsion (τ), and ontogeny axis length for all apertures (Okamoto, 1988; Harary & Tal, 2011). The local curvature and torsion, and accumulative ontogeny axis length were estimated from the aperture points along the growth trajectory by using weighted least-squares fitting and local arc length approximation (Lewiner et al., 2005). All the calculations were done with a custom-written Python script which can be implemented in Python interpreter in the Blender ver. 2.63 environment. The whole workflow was: (1) selecting the retopologised 3D shell Mesh (by clicking "right mouse button"), (2) input parameters for number of sample points "q = ##" in the python script, and (3) paste the script into the Python interpreter (Supplementary Information File 1). The final outputs with torsion, curvature and ontogeny axis reference for each aperture were saved as CSV files.

We found a convergence issue in curvature and torsion estimators. The accuracy of the curvature and torsion estimates depends on the number and density of the vertices in the ontogeny axis (i.e. number of aperture outlines), and the number of sample points. Nevertheless, different numbers of sample points can be adjusted until good (i.e. converged) curvature and torsion estimates are obtained. We used 10% of the total points as number of sample points of the ontogeny axis, which gave reasonably good estimates for curvature and torsion.

Notwithstanding the algorithm issue, the curvature and torsion estimators are informative in describing the shell spiral geometry growth trajectory. Curvature is always larger or equal to zero ($\kappa \geq 0$). When $\kappa = 0$, the spatial curve is a straight line; the larger the curvature, the smaller the radius of curvature ($1/\kappa$), and thus the more tightly coiled the spatial curve. On the other hand, the torsion estimator can be zero or take either negative or positive values ($-\infty \leq \tau \leq \infty$). When $\tau = 0$, the spatial curve lies completely in one plane (e.g. a flat planispiral shell), negative torsion values correspond to left-handed coiling and to right-handed coiling for positive torsion values; the larger the torsion, the smaller the radius of torsion ($1/\tau$), and thus the taller the spiral.

6. Quantifying aperture form

We quantified the aperture outline sizes as perimeter and form as normalised Elliptic Fourier coefficients (normalised EFA) by using a custom-written Python script which can be implemented Python interpreter embedded in the Blender environment. The workflow was (1) selecting the retopologised 3D shell mesh (by clicking "right mouse button"), (2) input parameters for "number_of_points_for_each_aperture = ##" in the python script, and (3) paste the script into the Python interpreter of Blender (Supplementary Information File 1). The final outputs were saved as CSV files.

Aperture outline perimeter was estimated from the sum of lengths (mm) for all the edges that are connecting the vertices (hereafter "aperture size"). For aperture form analysis, we used 3D normalised EFA algorithms (Godefroy et al., 2012) and implemented these in the custom python script. Although many algorithms exist for describing and quantifying the form of a closed outline (Claude, 2008), we used EFA because it is robust to unequally spaced points, can be normalised for size and orientation, and can capture complex outline form with a small number of harmonics (Rohlf & Archie, 1984; Godefroy et al., 2012). In this study, we used five harmonics, each with six coefficients which were sufficient to capture the diverse aperture shapes of our shells. For quantification of apertures shape that are invariant to size and rotation, we normalised EFA of aperture outlines for orientation and size. If needed for comparison with other studies, the normalised EFA can be repeated for the same dataset with higher or lower numbers of harmonics.

After normalisation, we ran principal components analysis (PCA) to summarise the 30 normalised Fourier coefficients as principal components scores (hereafter "aperture shape scores"). After that, we selected the major principal components (explaining > 90 % of the variance) for further analysis. The aperture shape scores of each selected principal component were plotted and analysed against the ontogeny axis.

7. Visualising aperture form and trajectory changes along the shell ontogeny

For exploration of data, we used two graphical techniques for representing aperture ontogeny profile changes along the shell ontogeny. For each shell, we made a vertical four-panels scatter plot in which each of the four variables (namely, curvature, torsion, aperture size, and the first principal component aperture shape score) were plotted against the ontogeny axis. When necessary, the second and third principal component aperture shape scores were also included. In

addition, the axis of each variable was rescaled so that it was the same for the same variable of all shells. After standardisation of the axis, the aperture ontogeny profiles of several shells could be quantitatively compared side by side.

However, comparison of between plots would become less effective with a larger number of shells. Alternatively, therefore, all aperture ontogeny profile variables of each shell can also be represented in a radar chart, instead of scatter plots. This chart is effective in showing the variable outliers within a chart and the overall similarity between charts. Before plotting the data in a radar chart, the datasets of all shells need to be restructured because the dataset of different shells could differ in the number of data points (i.e. quantified aperture), which depends on the ontogeny axis length of each shell.

We did this by dividing the ontogeny axis of each shell into 20 equal length intervals, and then by sampling the variable values at the end of every interval. In the restructured dataset, the trend of the aperture ontogeny profile of each variable is retained and all radar charts have the same number of data points. Thus, the changes of aperture variables between each subsequent 1/20 of the ontogeny axis can be examined within a shell and be compared among different shells in a synchronistic manner. We suggest to use 20 points to summarise hundreds variable points of the aperture ontogeny profile variables along ontogeny axis because the radar would be overwhelming with too many points and hard to interpret. Similar to the scatter plot, we standardised the axis scales of each variable of all radar charts.

In addition, we added a new variable which represents the ontogeny axis interval length in order to compensate for the loss of shell size information during the standardisation of ontogeny axis length. Finally, we plotted the variables, namely, curvature, torsion, aperture size, and ontogeny axis length, and aperture shape scores in a radar chart for each shell by using the "fmsb" library (Nakazawa, 2010) with R version 3.0.1 (R Core Team, 2013) (Supplementary Information File 3).

8. Quantitative comparison between shell forms

In addition to the qualitative comparison between shells forms as described above, the dissimilarity between different shells can be analysed quantitatively. We used Permutation Distribution Clustering (PDC) which finds similarities in a time series dataset (Brandmaier,

2012a; Brandmaier, 2012b). PDC can be used for the analysis of the changes in a variable along shell ontogeny between different shells (i.e. two-dimensional dataset: number of shells × number of apertures) and multiple variable changes between shells (i.e. three-dimensional dataset: number of shells × number of variables × number of apertures).

Although PDC is robust to the length differences between datasets, our preliminary analysis showed that the PDC output would be biased when there was a great (around two-fold) length difference in the total ontogeny axis length. Hence, we standardised the data as in procedure 7, but dividing the ontogeny axis of each shell into 50, instead of 20, equal length intervals. This standardisation procedure allows comparison of trends in variable changes along the shell ontogeny without the influences of size. In other words, the dissimilarity is zero between two shells that have exactly the same shape, but differ only in size. In addition to the shape comparison, we obtained the shell size in terms of volume by using "Volume" function in Blender after the 3D shell model was closed at both ends by creating faces "Make edge/Face") on selected apertures at both end ("Loop Select") in EDIT mode.

The aperture ontogeny profiles of all shells were combined into a three-dimensional data matrix consisting of n shells × four variables × 50 aperture data points. We ran four PDCs, each for the five data matrices with: 1) all four variables, 2) torsion, 3) curvature, 4) aperture size, and 5) aperture shape scores. The parameter settings for the PDC analysis were as follows: embedding dimension = 5; time-delay of the embedding = 1; divergence measure between discrete distributions = symmetric alpha divergence; and hierarchical clustering linkage method = single. The dissimilarity distances between shells were used to produce the dendrogram. PDC analysis was performed with the "pdc" library (Brandmaier, 2012b) in R version 3.0.1 (R Core Team, 2013) (Supplementary Information File 3).

In addition to the dendrogram representation of the output from PDC, we plotted the dissimilarity as a non-metric multidimensional scaling (NMDS) plot which resembles a morphospace. NMDS was performed by using "MASS" library (Venables & Ripley, 2002) in R version 3.0.1 (R Core Team, 2013) (Supplementary Information File 3).

Worked example: Comparative analysis of *Opisthostoma* species shell form and simulated shell form

We evaluated the above-described shell form quantification method by using the shells of *Opisthostoma*, which exhibit a great variability in shell form. Some of the species follow a regular coiling regime whereas others deviate from regular coiling in various degrees. It remains a challenging task to quantify and compare these shell forms among species, either by using traditional or geometric morphometrics, because a standard aperture view for the irregular and open coiled shells cannot be determined.

We selected four *Opisthostoma* species, namely, *Opisthostoma laidlawi* Skyes 1902 (Figure 2A), *Opisthostoma crassipupa* van Benthem Jutting, 1952 (Figure 2B), *Opisthostoma christae* Maassen 2001 (Figure 2C), and *Opisthostoma vermiculum* Clements and Vermeulen, 2008 (in Clements et al., 2008) (Figure 2D), for which the shell forms are, respectively: regularly coiled, slight distortion of the last whorl, strong distortion of the last whorl, and complete distortion of most of the whorls. We retopologised these four shells by following the procedures 1 to 4 (Supplementary Information Files 12).

In addition to the four retopologised 3D shell models, we manually created another four shell models by transforming three out of the four retopologised NURBS surface 3D shell models by using the "Transform" function in Blender. These models are: 1) *Opisthostoma laidlawi* that was resized to half the original size and given slight modification of the aperture size (Figure 2E); 2) *Opisthostoma christae* that was reshaped into an elongated form by reducing the model size (linear dimension) to one-half along the x and y axes, and by doubling the size along the z axis (Figure 2F); 3) *Opisthostoma christae* that was reshaped into a depressed form by multiplying by 1.5 the model size along the x and y axes, and by reducing to one-half along the z axis (Figure 2G); and 4) *Opisthostoma vermiculum* that consists of one *Opisthostoma vermiculum* original 3D model of which we connected the aperture to another, enlarged, *Opisthostoma vermiculum* (Figure 2H). Finally, we analysed all these eight shell models by following the procedures 5 to 8.

Results and Discussion

Retopologied 3D shell models

All the final retopologised 3D shell models can be found in Supplementary Information (Files 4 to 11) in PLY ASCII mesh format, with the raw data as a list of vertices, followed by a list of polygons, which can be accessed directly without the need of any 3D software. Each vertex is

represented by x, y, z coordinates. Each polygon face consists of four vertices. This simplified yet biologically informative 3D mesh shell model allows the quantification of aperture form and growth trajectory. Moreover, the 3D shell models and their raw vertices data could potentially be used in studies of functional morphology and theoretical modelling of shell form, respectively.

Malacologists have been focusing on empirical shell morphological data, from which the functional, ecological and evolutionary aspects were then extracted. The physical properties were then determined by its form (e.g. Okajima & Chiba 2011; Okajima & Chiba, 2012). By using the 3D models, the shell properties and function can be analysed *in silico*. For example, the thickness of the shell can be added to the 3D shell model (Figure 3E and Figure 3F) in order to obtain the shell material's volume, the shell's inner volume, its inner and outer surface area, and centre of gravity. Quantification of shell properties may then be done by using the geometry approach in Meshlab or Blender, as compared to the pre-3D era where mathematical descriptions of the shell form were required (e.g. Moseley, 1838; Raup & Graus, 1972; Stone, 1997). Furthermore, it is possible to convert the 3D models to a 3D finite element (FE) model, of which the physical properties (e.g. strength) can be tested (e.g. Faghih Shojaei et al., 2012).

In addition to the potential use of 3D shell models in functional morphology, the coordinate data of the vertices of 3D shell models could be used directly by theoretical morphologists (see Figure 1 in Urdy et al., 2010). For example, these data can be extracted in different formats that fit the data requirement of different types of theoretical shell models, namely, generating curve models using a fixed reference frame or moving reference frame (Figure 3C), helicospiral or multivector helicospiral models using a fixed reference frame (Figure 3A, Figure 3B and Figure 3D) or growth vector models using a moving reference frame (Figure 3A and Figure 3B).

The retopologising of the aperture ontogeny from a raw 3D shell model (procedures 1 to 4) is a time-consuming and tedious process compared with traditional and geometric morphometrics. For example, the four shell models were created by retopologising between 73 and 96 separate apertures. Nevertheless, the final product of a clean 3D shell mesh is versatile for many different kinds of analysis and thus has great potential for improving our understanding of shell form.

Comparing shell form from the view of shell ontogeny

Figure 4 gives an overview of the aperture ontogeny profile and shell volume for each species. The curvature, torsion perimeter, and ontogeny axis are represented by true numerical values with the unit of mm^{-1} and mm, and thus can be interpreted directly. In contrast, the aperture shape scores are just statistics of Fourier coefficients and are not the absolute quantification of aperture shape. The PCA score of an aperture shape depends on the shape of other aperture outlines and thus it might change whenever other aperture outlines are added into the analysis. Nevertheless, the aperture scores will stabilise as data of more shells become available and when most of the extreme aperture forms are included. In this study, the first principal component explained 92% of the total variance; the second and third principal component explained only 3% or 1% of the total variance. We showed that the shell form can be represented by the ontogeny changes of the aperture growth trajectory in terms of curvature and torsion, and aperture form, in terms of perimeter and shape.

Our first example evaluates this method in illustrating the differences between two shells that have the same shape but differ in shell size – the half-size *Opisthostoma laidlawi* (Figure 4E) shell and the original *Opisthostoma laidlawi* shell (Figure 4C). As revealed by their aperture ontogeny profiles, the size difference between the two shells has had an effect on the curvature, torsion, ontogeny axis length and aperture size. For the resized *Opisthostoma laidlawi* shell, the values of curvature and torsion are twice as large as for the original, whereas the ontogeny axis length and aperture size are only half those of the original shell. However, there is no discrepancy in the aperture shape statistics. Despite this scalar effect, the overall trends in the changes of these variables along the ontogeny axis are comparable between these two shells (Figure 6B).

Another example shows the ontogeny profiles of three shells, namely, the elongated (Figure 4G), depressed (Figure 4H), and original (Figure 4A) versions of the *Opisthostoma christae* shell. Comparison of aperture profiles among these show the most obvious discrepancies in greater torsion values for the elongated shell, which change in a more dramatic trend along the shell ontogeny. In addition, each of the three shells has its unique aperture shape scores, though there are no big discrepancies in the aperture size. The differences in ontogeny axis length, curvature and torsion are related to the differences of the aperture shape statistics among the three shells. However, our small dataset with only three shells is not sufficient for thorough disentangling of the interplay between aperture size, shape, and growth trajectory in relation to the shell form.

Our last example is the comparison between the original (Figure 4D) and the composite (Figure 4F) *Opisthostoma vermiculum* shell . It is clear that our method has high sensitivity and robustness in the analysis of such bizarre shell forms. As shown in Figure 4F, the start of the aperture ontogeny profile of the composite shell was the same as for the original shell (Figure 4D). In addition, the later parts of the ontogeny profile trends are still comparable to the first part, but different in value because of the scalar effect.

As an alternative visualisation, Figure 5 shows the radar charts that summarise the same aperture ontogeny profiles of each species. The polygon edges in each chart show how dramatically the aperture form (size and shape), and growth trajectory (curvature and torsion) are changing at each of the subsequent 5% intervals of the shell ontogeny. The aperture size (mm) and the ontogeny segment length (mm) variables indicate the shell size (i.e. volume). To illustrate this, aperture size and ontogeny axis length can be seen as the circle size and height of a cylinder. This chart is useful for the visual comparison between shells that are similar in size, for example, *Opisthostoma christae* (2.43 mm^3), *Opisthostoma laidlawi* (2.39 mm^3), and the depressed *Opisthostoma christae* (2.73 mm^3). The radar chart shows that (1) the depressed *Opisthostoma christae* is the largest and has a very different aperture shape as compared to the other two shells; (2) most of the shell whorls' form of *Opisthostoma christae* is very similar to *Opisthostoma laidlawi* (i.e. most of the polygons in the chart were similar), but the *Opisthostoma laidlawi* shell differs from *Opisthostoma christae* shell by having distorted whorls at the last part of the shell ontogeny (magenta lines at torsion) and a more open umbilicus at the beginning of the shell ontogeny (red lines at curvature and aperture size).

However, comparison of radar charts between shells that differ greatly in size would be less informative. For example, the radar charts between the resized *Opisthostoma laidlawi* shell and the original *Opisthostoma laidlawi* shell are very different, though the resized one has the same shell shape as the original. The difference in radar charts between the two shells was therefore mainly caused by the size difference.

As we have shown in both graphical techniques (Figures 4 and 5), the shell forms can be explored and compared qualitatively on the basis of aperture ontogeny profiles. Users might need some training in the interpretation of the plots because they are different from both linear dimension measurement plots and geometric morphometric shape coordinate plots. Our

evaluation suggested that both data visualisation methods are sensitive and robust in capturing the aperture ontogeny profile for any shell form and thus make the qualitative comparison across gastropod taxa and studies possible.

This method could be applied in malacological taxonomy because its core business is the description of shell form. Despite hundreds of years of taxonomic history of shells, there has been little change in the way shell form is being described. For example, shell from is usually described in terms of linear dimensions: shell width and height; number of whorls; shell shape – flat, depressed, globose, conical, or elongated; whorls shape – from flat to convex. Here, we suggest that the aperture ontogeny profiles would be a great supplement to the classical approach to shell description. For example: (1) the size of the shell (its volume) depends on the ontogeny axis length and aperture size; (2) the shell shape depends on the growth trajectory in terms of curvature and torsion; (3) the shape of the whorls depends on the shape of the aperture (Figure 4). In our case of the four *Opisthostoma* shells (Figures 2A – 2D), it is clear that aperture size of each shell is constricted at roughly the same part of the respective shell ontogeny, namely between 70% and 85%, regardless of the dissimilar shell sizes and shapes (Figures 4A – 4D, and aperture size profiles in Figure 5B). This suggests that the constriction in aperture size profile is a diagnostic character for the genus *Opisthostoma*. In the light of this example, we believe that these aperture ontogeny profiles could aid the taxonomist in decision-making for grouping taxa based on homologous characters.

Quantitative comparison between different shell forms

Figure 6 shows dendrograms resulting from a permutation distribution clustering analysis of the eight shells in terms of their aperture ontogeny profiles. Figure 6A shows the hierarchical clustering of the eight shells based on all four aperture ontogeny profiles. From this dendrogram, the composite *Opisthostoma vermiculum* is completely separate from the other shells. The remaining seven shells are clustered into two groups. One consists of the more regularly coiled shells, namely, *Opisthostoma christae* and its two transformed shells, and *Opisthostoma crassipupa*; the other group consists of the shells that deviate from regular coiling, namely *Opisthostoma laidlawi* and its transformed shell, and *Opisthostoma vermiculum*. Nevertheless, there were high dissimilarities between shells within each group as revealed by the long branch lengths in Figure 6A, except for the two *Opisthostoma laidlawi* shells (Table 1). The aperture ontogeny profiles for the *Opisthostoma laidlawi* shell and its reduced version are almost the

same. The high dissimilarity among the other six shells can be explained when each of the variables in the aperture ontogeny profile is analysed separately as shown in Figure 6B.

Figure 6B shows the dendrograms of aperture ontogeny profiles for each of the four variables. All four dendrograms have a different topology than the one in Figure 6A. Among the variables, the aperture ontogeny profile of the curvature has the smallest discrepancies among shells. The two *Opisthostoma laidlawi* shells are the only pair that clusters together in all the dendrograms of Figures 6A and 6B because they are identical in every aspect of aperture ontogeny profile except torsion. Hence, the independent analysis of aperture ontogeny profile variables corresponds well to the overall analysis of aperture ontogeny profiles.

Figure 7 shows a three-dimensional NMDS plot of the distance matrix (Table 1) that was generated from PDC analysis on all four aperture ontogeny profiles. The very low stress level (0.000) indicates that this 3D plot is sufficient to represent the distance matrix of the aperture ontogeny profiles. This NMDS plot can therefore be regarded as a morphospace of the shell shape, as derived from aperture ontogeny profiles. However, neither the dendrogram nor the NMDS plot contains information about the shell size because the analysis of PDC is based on the standardised ontogeny profiles and their trends. Thus, both plots are useful for the comparative analysis of shell shape, but not shell size. Nevertheless, the size comparison between shells is rather straightforward.

The conventional quantification of shell size is based on the linear measurement of two or three dimensions of a shell, for example, shell height and shell width. However, shell size may be more appropriately given as shell volume, which can be estimated easily from retopologised 3D shell models (Figure 4). A shorthand to qualitatively comparing size between two shells is by examining the ontogeny axis length and aperture size in the radar chart (Figure 5). We can then compare the form between shells when the dendrograms or NMDS plot are interpreted together with shell size (volume) data. For example, the *Opisthostoma laidlawi* shell has the same shape as, but is eight times larger than, the resized *Opisthostoma laidlawi*.

In addition to the construction of morphospace, the dissimilarity matrix can be used in phylogenetic signal tests (Hardy & Pavoine, 2012). Furthermore, it can also be analysed together

with other distance matrices, such as for geographical or ecological distance, to improve our understanding of the evolutionary biology of shell forms.

Conclusions, limitations and future directions

We demonstrated an alternative workflow for data acquisition, exploration and quantitative analysis of shell form. This method has several advantages over traditional and geometric morphometrics in the analysis of shell forms, namely in terms of: (1) robustness – this method can be used to compare any shell form; (2) scalability and reproducibility – the data obtained from different studies and different gastropod taxa can be integrated; (3) versatility – the raw 3D shell mesh models, coordinates data of the vertices, aperture ontogeny profiles, and dissimilarity matrix between shell forms can be used for taxonomy, functional morphology, theoretical modelling, and evolutionary studies.

Yet, our method has its limitations. Firstly, our retopology procedures rely on a 3D shell model that requires CT-scan technology. In fact, although a CT-scan 3D shell model can certainly facilitate the retopology process of a shell, it is not indispensable. The key of the retopology processes is to digitise the aperture along the shell ontogeny, and thus a shell can be retopologised fully in Blender with a good understanding of the aperture ontogeny profiles by studying the real specimens even without a reference shell model. Secondly, the retopology procedure which is essential for our data acquisition is more time-consuming than traditional and geometric morphometric where data can be obtained from an image taken from a shell. Thirdly, our method is effective in the analysis of overall shell form, but not of the shell ornamentation.

In the future, our method can be improved to accommodate the shell ornamentation analysis. Parts of our method (i.e. procedures 1 – 6) can be used to obtain shell ornamentation data, such as radial ribs (*i.e.,* commarginal ribs), but these data cannot be analysed with our qualitative and quantitative approaches that focus on longitudinal growth (i.e. procedures 7 – 8). Finally, we hope this shell form quantification method will simulate more collaboration within malacologists that work in different research fields, and between empirical and theoretical morphologists.

Supplementary Information (http://dx.doi.org/10.6084/m9.figshare.877061)

File S1– A python script for procedures 5 and 6 – Aperture form and growth trajectory analysis on retopologised 3D shell mesh in Blender.

File S2– A python script to convert normalised elliptical Fourier coefficients to polygon mesh in Blender.

File S3 – An R script for data analysis as described in procedures 7 and 8.

File S4 – PLY ASCII mesh 3D model of *Opisthostoma laidlawi* Sykes 1902.

File S5 – PLY ASCII mesh 3D model of *Opisthostoma crassipupa* van Benthem Jutting, 1952.

File S6 – PLY ASCII mesh 3D model of *Opisthostoma christae* Maassen 2001.

File S7 – PLY ASCII mesh 3D model of *Opisthostoma vermiculum* Clements and Vermeulen, 2008.

File S8 – PLY ASCII mesh 3D model of *Opisthostoma laidlawi* that was reduced in size by one-half and with slight modification of the last aperture size.

File S9 – PLY ASCII mesh 3D model of *Opisthostoma christae* that was reshaped into an elongated form by reducing the model size (linear dimension) by one-half along the x and y axes, and by doubling the size along the z axis.

File S10 – PLY ASCII mesh 3D model of *Opisthostoma christae* that was reshaped into a depressed form by doubling the model size along the x and y axes, and by reducing the size by one-half along the z axis.

File S11 – PLY ASCII mesh 3D model of *Opisthostoma vermiculum* that consists of one *Opisthostoma vermiculum* original 3D model of which the aperture was connected to a second enlarged *Opisthostoma vermiculum*.

File S12 – A Blender file consisting of raw data of 8 shells of procedures 1 – 4.

Acknowledgments

We are thankful to Heike Kappes, Ton de Winter, Jaap Vermeulen, and Severine Urdy for fruitful discussion. We are grateful to Willem Renema for introducing LTS to CT-Scan instrumentation. Finally, we would like to acknowledge ## anonymous reviewers for providing useful comments that improved the manuscript.

Author Contributions

Conceived and designed the experiments: LTS. Performed the experiments: LTS. Analyzed the data: LTS. Contributed reagents/materials/analysis tools: LTS MS. Wrote the paper: LTS MS.

References

Abel RL, Laurini CR, Richter M. 2012. A palaeobiologist's guide to 'virtual'micro-CT preparation. *Palaeontologia Electronica* 15(2):1-16.

Ackerly SC. 1989a. Kinematics of accretionary shell growth, with examples from brachiopods and molluscs. *Paleobiology* 15(2):147-164.

Ackerly SC. 1989b. Shell coiling in gastropods: analysis by stereographic projection. *Palaios* 4:374-378

Andrei RM, Callieri M, Zini MF, Loni T, Maraziti G, Pan MC, Zoppè M. 2012. Intuitive representation of surface properties of biomolecules using BioBlender. *BMC Bioinformatics*, 13(Suppl 4):S16.

Atwood JW, Sumrall CD. 2012. Morphometric investigation of the Pentremites fauna from the Glen Dean formation, Kentucky. *Journal of Paleontology* 86(5):813-828.

Bayer U. 1978. Morphogenetic programs, instabilities and evolution: a theoretical study. *Neues Jahrbuch für Geologie und Paläontologie. Abhandlungen* 156:226-261.

van Benthem-Jutting WSS. 1952. The Malayan species of *Opisthostoma* (Gastropoda, Prosobranchia, Cyclophoridae), with a catalogue of all the species hitherto described. *The Bulletin of the Raffles Museum* 24(5):5-61.

Van Bocxlaer B, Schultheiß R. 2010. Comparison of morphometric techniques for shapes with few homologous landmarks based on machine-learning approaches to biological discrimination. *Paleobiology* 36(3):497-515.

Boettiger A, Ermentrout B, Oster G. 2009. The neural origins of shell structure and pattern in aquatic mollusks. *Proceedings of the National Academy of Sciences* 106(16):6837-6842.

Bookstein FL. 1991. *Morphometric Tools for Landmark Data: Geometry and Biology*. Cambridge University Press.

Brandmaier AM. 2012a. *Permutation Distribution Clustering and Structural Equation Model Trees.* Fakultät 6 - Naturwissenschaftlich-Technische Fakultät I, Universität des Saarlandes.

Brandmaier AM. 2012b. *pdc: Permutation Distribution Clustering. R package version 0.3.* http://CRAN.R-project.org/package=pdc

Cain AJ. 1977. Variation in the spire index of some coiled gastropod shells, and its evolutionary significance. *Philosophical Transactions of the Royal Society of London. B, Biological Sciences* 277:377-428

Cardini A, Loy A. 2013. On growth and form in the" computer era": from geometric to biological morphometrics. *Hystrix, the Italian Journal of Mammalogy,* 24(1), 1-5.

Cassola, VF, de Melo Lima VJ, Kramer R, Khoury HJ. 2010. FASH and MASH: female and male adult human phantoms based on polygon mesh surfaces: I. Development of the anatomy. *Physics in Medicine and Biology* 55(1):133.

Chaplin TA, Yu HH, Rosa MG. 2013. Representation of the visual field in the primary visual area of the marmoset monkey: Magnification factors, point-image size, and proportionality to retinal ganglion cell density. *Journal of Comparative Neurology* 521(5):1001-1019.

Chacon R. 2012. Using Jacobian elliptic functions to model natural shapes. *International Journal of Bifurcation and Chaos* 22(1):1230005.

Checa A. 1991. Sectorial expansion and shell morphogenesis in molluscs. *Lethaia* 24(1):97-114.

Checa A, Aguado R. 1992. Sectorial-expansion analysis of irregularly coiled shells: application to the recent gastropod *Distorsio*. *Palaeontology* 35:913-925.

729 Cignoni P, Corsini M, Ranzuglia G. 2008. Meshlab: an open-source 3d mesh processing system.
730 *Ercim news* 73:45-46.

731 Clarke RK, Grahame J, Mill PJ. 1999. Variation and constraint in the shells of two sibling species
732 of intertidal rough periwinkles (Gastropoda: *Littorina* spp.). *Journal of Zoology* 247(2):145-154.

733 Clements R, Liew TS, Vermeulen JJ, Schilthuizen M. 2008. Further twists in gastropod shell
734 evolution. *Biology letters* 4(2):179-182.

735 Claude J. 2008. *Morphometrics with R*. Springer.

736 Cortie MB. 1989. Models for mollusk shell shape. *South African Journal of Science* 85(7):454-
737 460.

738 Cortie MB. 1993. Digital seashells. *Computers & graphics* 17(1):79-84.

739 Davoli E, Russo F. 1974. Una metodologia paleontometrica basata sul modello di Raup: Verifica
740 sperimentale su rappresentanti follili del gen. *Subula* Schumacher. *Bollettino della Societa*
741 *Paleontologica Italiana* 13:108-121.

742 Dera G, Eble GJ, Neige P, David B. 2009. The flourishing diversity of models in theoretical
743 morphology: from current practices to future macroevolutionary and bioenvironmental
744 challenges. *Paleobiology* 34 (3):301-317.

745 Ekaratne SUK, Crisp DJ. 1983. A geometric analysis of growth in gastropod shells, with
746 particular reference to turbinate forms. *Journal of the Marine Biological Association of the*
747 *United Kingdom* 63(4):777-797.

748 Emberton K. 1994. Polygyrid land snail phylogeny: external sperm exchange, early North
749 American biogeography, iterative shell evolution. *Biological Journal of the Linnean Society*
750 52(3): 241-271.

751 Evans AR. 2013. Shape descriptors as ecometrics in dental ecology. *Hystrix, the Italian Journal*
752 *of Mammalogy*, *24*(1), 8.

753 Faghih Shojaei M, Mohammadi V, Rajabi H, Darvizeh A. 2012. Experimental analysis and
754 numerical modeling of mollusk shells as a three dimensional integrated volume. *Journal of the*
755 *Mechanical Behavior of Biomedical Materials* 16:38-54.

756 Foote M, Cowie RH. 1988. Developmental Buffering as a Mechanism for Stasis: Evidence from
757 the Pulmonate *Theba pisana*. *Evolution* 42(2):396-399.

758 Fowler DR, Meinhardt H, Prusinkiewicz P. 1992. Modeling seashells. *ACM SIGGRAPH*
759 *Computer Graphics* 26(2):379-387.

760 Galbraith C, Prusinkiewicz P, Wyvill B. 2002. Modeling a *Murex cabritii* sea shell with a
761 structured implicit surface modeler. *The Visual Computer* 18(2):70-80.

762 Godefroy JE, Bornert F, Gros CI, Constantinesco A. 2012. Elliptical Fourier descriptors for
763 contours in three dimensions: A new tool for morphometrical analysis in biology. *Comptes*
764 *rendus biologies* 335(3):205-213.

765 Goodfriend GA. 1983. Some new methods for morphometric analysis of gastropod shells.
766 *Malacological Review* 16:79-86.

767 Graus RR. 1974. Latitudinal trends in the shell characteristics of marine gastropods. *Lethaia*,
768 *7*(4):303-314.

769 Hardy OJ, Pavoine S. 2012. Assessing phylogenetic signal with measurement error: a comparison
770 of Mantel tests, Blomberg et al.'s K, and phylogenetic distograms. *Evolution* 66:2614-2621

771 Haug JT, Maas A, Waloszek D. 2009. Ontogeny of two Cambrian stem crustaceans, †*Goticaris*
772 *longispinosa* and †*Cambropachycope clarksoni*. *Palaeontographica A* 289:1-43.

773 Haug JT, Waloszek D, Haug C, Maas A. 2010. High-level phylogenetic analysis using
774 developmental sequences: The Cambrian †*Martinssonia elongata*, †*Musacaris gerdgeyeri* gen. et
775 sp. nov. and their position in early crustacean evolution. *Arthropod Structure & Development*
776 39(2):154-173.

777 Haug C, Haug JT, Fayers SR, Trewin NH, Castellani C, Waloszek D, Maas A. 2012.
778 Exceptionally preserved nauplius larvae from the Devonian Windyfield chert, Rhynie,
779 Aberdeenshire, Scotland. *Palaeontologia Electronica* 15:2-24.

780 Harary G, Tal A. 2011. The natural 3D spiral. *Computer Graphics Forum* 30(2):237-246.

781 Hutchinson J. 1999. But which morphospace to choose?: Theoretical Morphology by GR
782 McGhee, Jr. *Trends in Ecology & Evolution* 14:414.

783 Iller C. 1983. The mathematics of gnomonic seashells. *Mathematical Biosciences* 63:21-56.

784 Illert C, Pickover CA. 1992. Generating irregularly oscillating fossil seashells. *Computer*
785 *Graphics and Applications, IEEE* 12(3):18-22.

786 Im CH, Park JH, Shim M, Chang WH, Kim YH. 2012. Evaluation of local electric fields
787 generated by transcranial direct current stimulation with an extracephalic reference electrode
788 based on realistic 3D body modeling. *Physics in Medicine and Biology* 57(8):2137.

789 Johnston MR, Tabachnick RE, Bookstein FL. 1991. Landmark-based morphometrics of spiral
790 accretionary growth. *Paleobiology* 17(1):19-36.

791 Kaesler RL, Waters JA. 1972. Fourier analysis of the ostracode margin. *Geological Society of*
792 *America Bulletin* 83(4):1169-1178.

793 Kawaguchi Y. 1982. A morphological study of the form of nature. *Computer Graphics* 16:223-
794 232.

795 Klingenberg CP. 2013. Visualizations in geometric morphometrics: how to read and how to make
796 graphs showing shape changes. *Hystrix, the Italian Journal of Mammalogy, 24(1)*, 10.

797 Kohn AJ, Riggs AC. 1975. Morphometry of the *Conus* shell. *Systematic Zoology* 24:346-359.

798 Kuhl FP, Giardina CR. 1982. Elliptic Fourier features of a closed contour. *Computer Graphics*
799 *and Image Processing* 18(3):236-258.

800 Lewiner T, Gomes Jr JD, Lopes H, Craizer M. 2005. Curvature and torsion estimators based on
801 parametric curve fitting. *Computers & Graphics* 29(5):641-655.

802 Liew TS, Kok ACM, Urdy S, Schilthuizen M. in press-b. On shell growth and form of a
803 heteromorphic terrestrial snail: *Opisthostoma concinnum* Fulton, 1901 (Mollusca: Gastropoda:
804 Diplommatinidae).

805 Løvtrup S, von Sydow B. 1974. D'Arcy Thompson's theorems and the shape of the molluscan
806 shell. *Bulletin of Mathematical Biology* 36:567-575.

807 Lv Z, Tek A, Da Silva F, Empereur-mot C, Chavent M, Baaden M. 2013. Game On, Science-How
808 Video Game Technology May Help Biologists Tackle Visualization Challenges. *PLoS ONE*
809 8(3):e57990.

810 Maassen WJM. 2001. Four new Diplommatinidae (Gastropoda, Prosobranchia,
811 Diplommatinidae) from southern Thailand and northern Peninsular Malaysia. *Basteria* 65(1-
812 3):51-56.

813 Mayer G, Haug J, Maas A, Waloszek D. 2012. Functional aspects of the gammaridean mandibles
814 with special reference to the lacinia mobilis (Crustacea, Amphipoda). *Zoologischer Anzeiger-A*
815 *Journal of Comparative Zoology* 252:536-547.

816 McGhee GR. 1978. Analysis of the shell torsion phenomenon in the Bivalvia. *Lethaia* 11(4):315-
817 329.

McGhee GR. 1999. *Theoretical Morphology: the Concept and Its Applications*. Columbia University Press.

McGhee GR. 2007. *The Geometry of Evolution: Adaptive Landscapes and Theoretical Morphospaces*. New York: Cambridge University Press.

Meinhardt H. 2009. *The Algorithmic Beauty of Sea Shells*. Springer.

Monnet C, Zollikofer C, Bucher H, Goudemand N. 2009. Three-dimensional morphometric ontogeny of mollusc shells by micro-computed tomography and geometric analysis. *Paleontologia Electronica* 12(3/12A):1-13.

Moseley H. 1838. On the geometrical forms of turbinated and discoid shells. *Philosophical Transactions of the Royal Society of London* 128:351-370.

Moulton DE, Goriely A. 2012. Surface growth kinematics via local curve evolution. *Journal of mathematical biology*: 1-28.

Moulton DE, Goriely A, Chirat R. 2012. Mechanical growth and morphogenesis of seashells. *Journal of Theoretical Biology* 311:69-79.

Nakazawa M. 2012. *fmsb: Functions for Medical Statistics Book with Some Demographic Data. R package version 0.4.1.* http://CRAN.R-project.org/package=fmsb

Newkirk GF, Doyle RW. 1975. Genetic analysis of shell-shape variation in *Littorina saxatilis* on an environmental cline. *Marine Biology* 30(3):227-237.

Noshita K. 2010. Spiral Shell Form: A computer software package for theoretical morphological analysis of spiral shell form. *Geoscience reports of Shizuoka University* 37:57-73. (In Japanese)

Okajima R, Chiba S. 2011. How does life adapt to a gravitational environment? The outline of the terrestrial gastropod shell. *The American Naturalist* 178(6):801-809.

840 Okajima R, Chiba S. 2012. Adaptation from restricted geometries: the shell inclination of
841 terrestrial gastropods. *Evolution* 67:429-437.

842 Okamoto T. 1988. Analysis of heteromorph ammonoids by differential geometry. *Palaeontology*
843 31(1):35-52.

844 Oliphant TE. 2007. Python for scientific computing. *Computing in Science & Engineering*
845 9(3):10-20.

846 Picado J. 2009. Seashells: the plainness and beauty of their mathematical description. *MAA*
847 *Mathematical Sciences Digital Library*: 1-18.

848 Pyka M, Hertog M, Fernandez R, Hauke S, Heider D, Dannlowski U, Konrad C. 2010. fMRI data
849 visualization with BrainBlend and Blender. *Neuroinformatics* 8(1):21-31.

850 R Core Team. 2013. *R: A Language and Environment for Statistical Computing*. R Foundation
851 for Statistical Computing, Vienna, Austria. URL http://www.R-project.org/.

852 RStudio. 2012. *RStudio: Integrated Development Environment for R* (Version 0.97.336), Boston,
853 MA. URL http://www.rstudio.org/.

854 Raup DM. 1961. The geometry of coiling in gastropods. *Proceedings of the National Academy of*
855 *Sciences of the United States of America* 47(4):602.

856 Raup DM. 1967. Geometric analysis of shell coiling: coiling in ammonoids. *Journal of*
857 *Paleontology* 41(1):43-65.

858 Raup DM, Graus RR. 1972. General equations for volume and surface area of a logarithmically
859 coiled shell. *Journal of the International Association for Mathematical Geology* 4:307-316.

860 Raup DM, Michelson A. 1965. Theoretical morphology of the coiled shell. *Science*
861 147(3663):1294-1295.

862 Rice SH. 1998. The bio-geometry of mollusc shells. *Paleobiology* 24(1):133-149.

863 Rohlf FJ, Archie JW. 1984. A comparison of Fourier methods for the description of wing shape in
864 mosquitoes (Diptera: Culicidae). *Systematic Biology* 33(3):302-317.

865 Rohlf FJ, Slice D. 1990. Extensions of the Procrustes method for the optimal superimposition of
866 landmarks. *Systematic Biology* 39(1):40-59.

867 Samadi S, David P, Jarne P. 2000. Variation of shell shape in the clonal snail *Melanoides*
868 *tuberculata* and its consequences for the interpretation of fossil series. *Evolution* 54(2):492-502.

869 Sarkar D. 2008. *Lattice: Multivariate Data Visualization with R*. Springer.

870 Saunders WB, Shapiro EA. 1986. Calculation and simulation of ammonoid hydrostatics.
871 *Paleobiology* 12(1):64-79.

872 Savazzi E. 1985. SHELLGEN: A BASIC program for the modeling of molluscan shell ontogeny
873 and morphogenesis. *Computers & Geosciences* 11(5):521-530.

874 Savazzi E. 1990. Biological aspects of theoretical shell morphology. *Lethaia* 23(2):195-212.

875 Savazzi E. 1992. Shell construction, life habits and evolution in the gastropod *Velates*.
876 *Palaeogeography, Palaeoclimatology, Palaeoecology* 99(3):349-360.

877 Savazzi E. 1993. C++ classes for theoretical shell morphology. *Computers & Geosciences* 19(7):
878 931-964.

879 Savazzi E. 1995. Theoretical shell morphology as a tool in construction morphology. *Neues*
880 *Jahrbuch für Geologie und Paläontologie. Abhandlungen* 195:229-240.

881 Schindel DE. 1990. Unoccupied morphospace and the coiled geometry of gastropods:
882 architectural constraint or geometric covariation. In Ross, R. M. and Allmon W. D. (eds) *Causes*

883 *of Evolution: A Paleontological Perspective*. University of Chicago Press, Chicago. Page 270-
884 304.

885 Sykes ER. 1902. Descriptions of six new land shells from the Malay Peninsula. *Journal of*
886 *Malacology* 9:22-23.

887 Stępień C. 2009. An IFS-based method for modelling horns, seashells and other natural forms.
888 *Computers & Graphics* 33(4):576-581.

889 Stone JR. 1997. Mathematical determination of coiled shell volumes and surface areas. *Lethaia*
890 30:213-219.

891 Tissot BN. 1988. Geographic variation and heterochrony in two species of cowries (genus
892 *Cypraea*). *Evolution* 42(1):103-117.

893 Ubukata T. 2001. Stacking increments: a new model and morphospace for the analysis of bivalve
894 shell growth. *Historical Biology: A Journal of Paleobiology* 15(4):303-321.

895 Urdy S, Goudemand N, Bucher H, Chirat R. 2010. Allometries and the morphogenesis of the
896 molluscan shell: a quantitative and theoretical model. *Journal of Experimental Zoology Part B:*
897 *Molecular and Developmental Evolution* 314(4):280-302.

898 Venables WN, Ripley BD. 2002. *Modern Applied Statistics with S*. Springer.

899 Verduin A. 1982. How complete are diagnoses of coiled shells of regular build? A mathematical
900 approach. *Basteria* 45(6):127-142.

901 Vermeij GJ. 1971. Gastropod evolution and morphological diversity in relation to shell geometry.
902 *Journal of Zoology* 163(1):15-23.

903 Warburton K. 1979. Variation in shell geometry in the genus *Lacuna* (Prosobranchia: Lacunidae).
904 *Journal of Natural History* 13(3):385-391.

Table 1(on next page)

Table 1. Dissimilarity matrix of aperture ontogeny profiles of eight shells obtained from Permutation Distribution Clustering.

Table 1. Dissimilarity matrix of aperture ontogeny profiles of eight shells obtained from Permutation Distribution Clustering.

Shell	(1)	(2)	(3)	(4)	(5)	(6)	(7)	(8)
(1) *Opisthostoma laidlawi*	0,00							
(2) *Opisthostoma crassipupa*	2,44	0,00						
(3) *Opisthostoma christae*	2,65	2,83	0,00					
(4) *Opisthostoma vermiculum*	2,63	2,56	2,59	0,00				
(5) half-sized *Opisthostoma laidlawi*	2,69	2,80	0,09	2,55	0,00			
(6) composite *Opisthostoma vermiculum*	3,12	3,48	3,40	3,39	3,34	0,00		
(7) elongated *Opisthostoma christae*	2,09	2,55	3,03	2,79	3,03	3,36	0,00	
(8) depressed *Opisthostoma christae*	2,01	2,73	3,16	2,94	3,21	3,84	2,62	0,00

Figure 1

Procedures to generate a retopologised shell based on the aperture ontogeny from a shell by using Blender software.

(A) Procedure 3 - Creating reference: Tracing aperture from shell model. (B) Procedure 3 - Creating reference: Tracing ontogeny axis. (C) Procedure 3 – both traced aperture outline and ontogeny axis were converted to Bezier curves. (D) Procedure 4 – Retopologising aperture outlines from the reference by using NURBS circles in EDIT mode. (E) Retopologised aperture outlines. (F) Procedure 4 – Generating retopologised shell surface models from NURBS circles in EDIT mode. (G) Final retopologised NURBS surface shell model. (H) Retopologised 3D shell mesh converted from retopologised NURBS surface shell model.

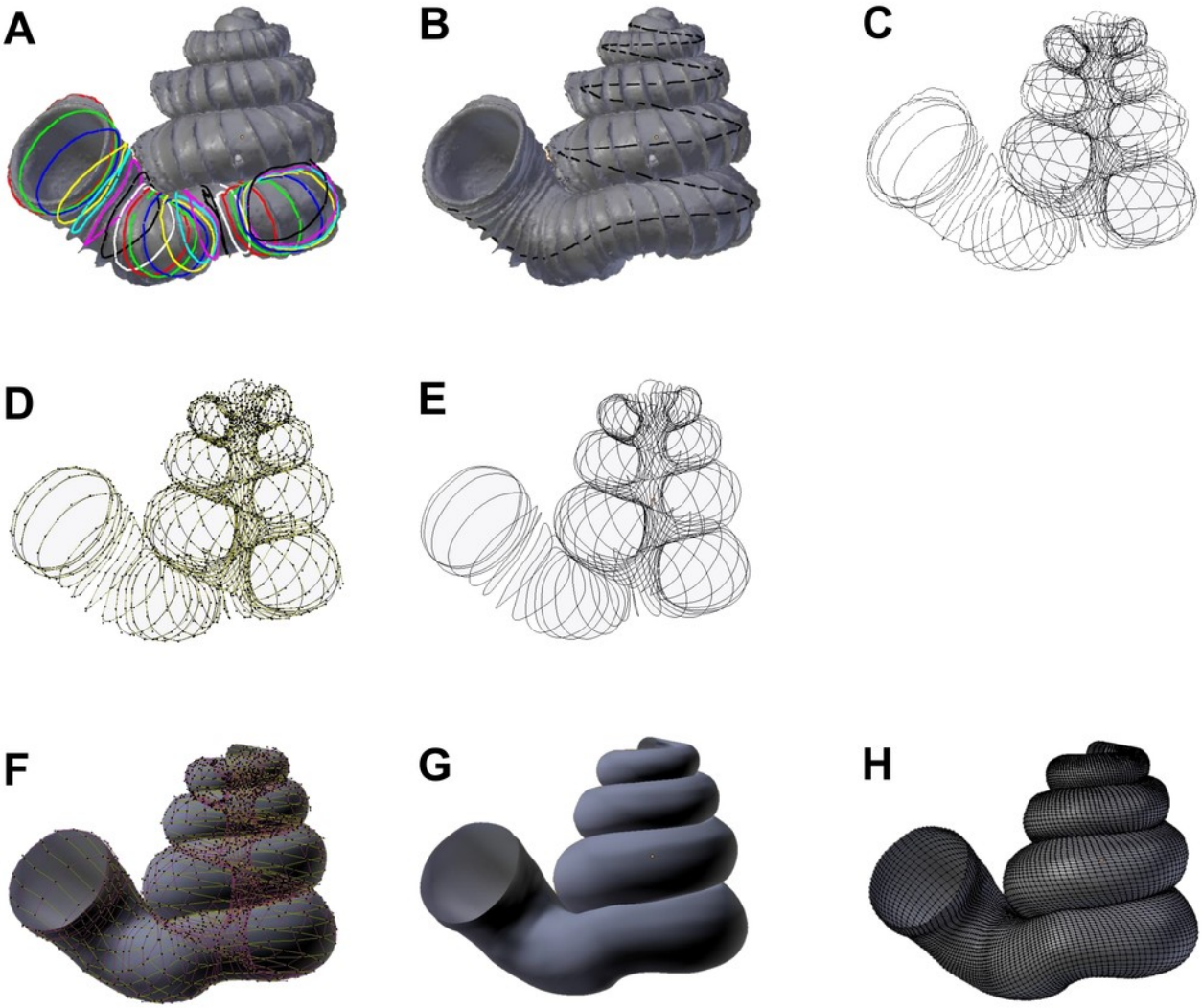

Figure 2

Retopologised shell 3D models obtained by repotologising real shells (A – D) and by transformation of retopologised shells (E – H).

(A) Shell of *Opisthostoma laidlawi* Sykes 1902. (B) Shell of *Opisthostoma crassipupa* van Benthem Jutting, 1952. (C) Shell of *Opisthostoma christae* Maassen 2001. (D) Shell of *Opisthostoma vermiculum* Clements and Vermeulen, 2008. (E) *Opisthostoma laidlawi* shell that was resized by one-half and with slight modification of the last aperture size. (F) *Opisthostoma christae* shell that was reshaped into an elongated form by reducing the model size (linear dimension) by one-half along the x and y axes, and by doubling the size along the z axis. (G) *Opisthostoma christae* shell that was reshaped into a depressed form by increasing by 1.5 the model size along the x and y axes, and by reducing the size by one-half along the z axis. (H) *Opisthostoma vermiculum* shell that consists of one *Opisthostoma vermiculum* original 3D model of which the aperture was connected to a second, enlarged, *Opisthostoma vermiculum*.

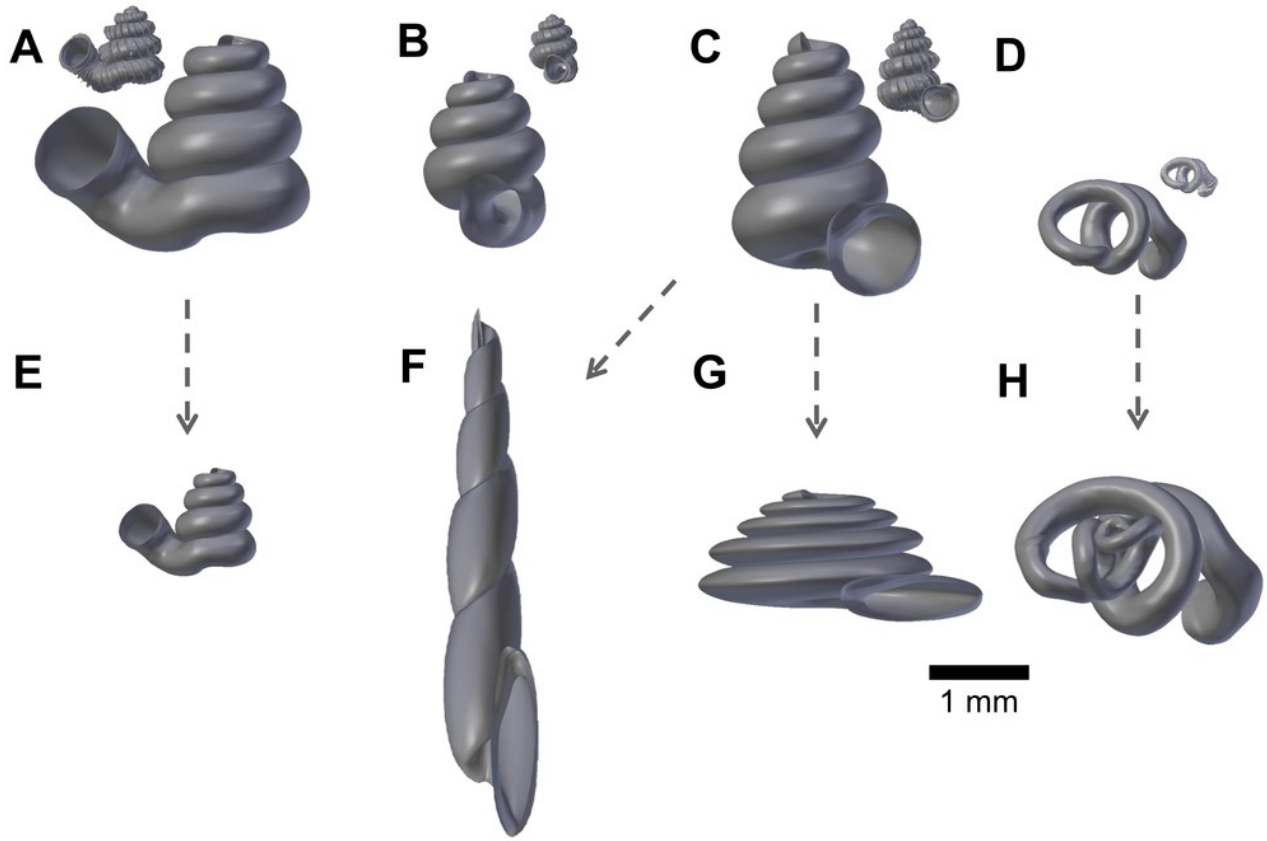

Figure 3

Different data types that could be obtained directly from a 3D shell model that was retopologised on the basis of the aperture ontogeny.

(A) Aperture maps (*sensu* Rice, 1998) or growth vector maps (*sensu* Urdy et al., 2010). (B) same as (A), but the data can be obtained in a greater resolution. (C) Aperture outlines data for generating curve models. (D) Multiple ontogeny axes for helicospiral models. (E) Simple 3D surface shell model with no thickness. (F) 3D surface shell model with added thickness.

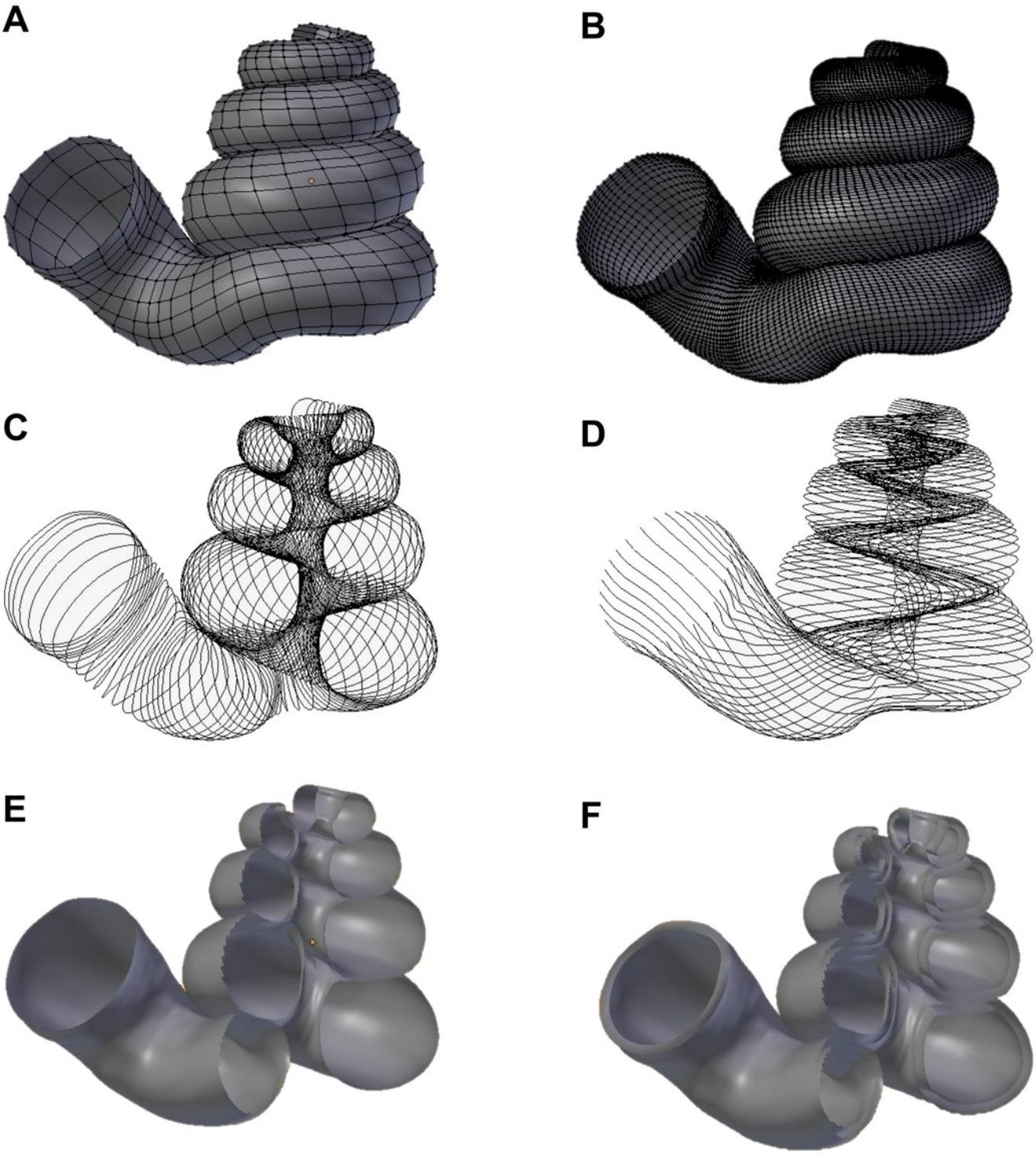

Figure 4

Shell size (volume) and aperture ontogeny profiles in terms of aperture growth trajectory (curvature and torsion) and aperture form (size and shape) of eight shells.

(A) Shell of *Opisthostoma laidlawi* Sykes 1902. (B) Shell of *Opisthostoma crassipupa* van Benthem Jutting, 1952. (C) Shell of *Opisthostoma christae* Maassen 2001. (D) Shell of *Opisthostoma vermiculum* Clements and Vermeulen, 2008. (E) *Opisthostoma laidlawi* shell that was resized by one-half and with slight modification of the last aperture size. (F) *Opisthostoma christae* shell that was reshaped into an elongated form by reducing the model size (linear dimension) by one-half along the x and y axes, and by doubling the size along the z axis. (G) *Opisthostoma christae* shell that was reshaped into a depressed form by increasing by 1.5 of the model size along the x and y axes, and by reducing the size by one-half along the z axis. (H) *Opisthostoma vermiculum* shell that consists of one *Opisthostoma vermiculum* original 3D model of which the aperture was connected to a second enlarged *Opisthostoma vermiculum*.

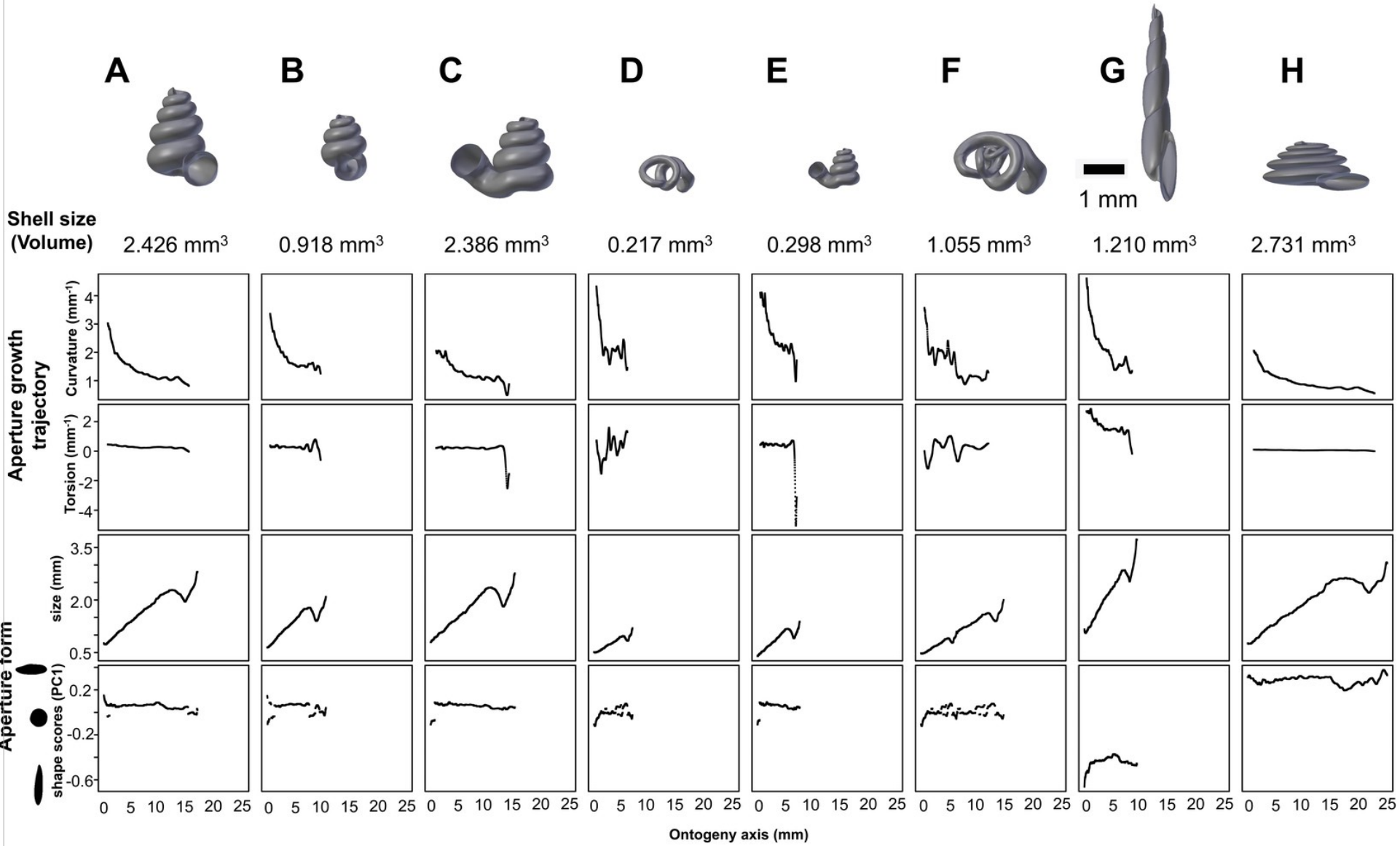

PeerJ PrePrints | https://peerj.com/preprints/157v1/ | v1 received: 16 Dec 2013, published: 16 Dec 2013, doi: 10.7287/peerj.preprints.157v1

Figure 5

Radar charts of the aperture ontogeny profiles of eight shells.

Each radar chart shows the value and trends of the curvature, torsion, aperture size, aperture shape scores, and ontogeny axis length of each shell.

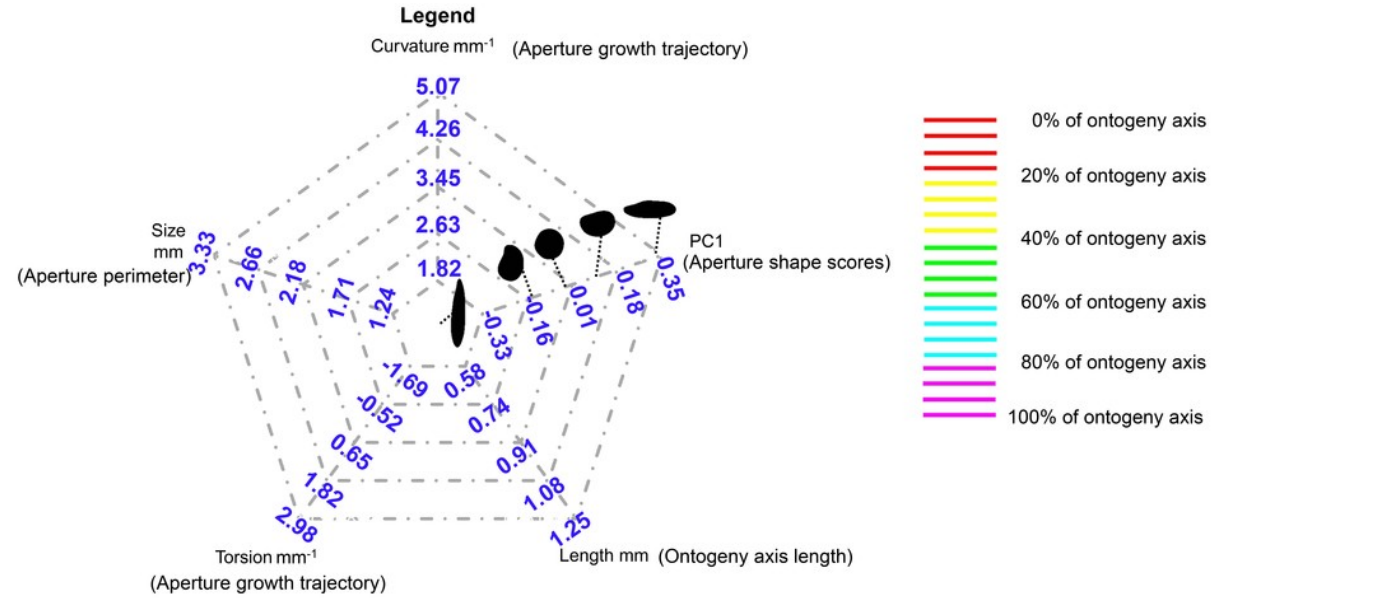

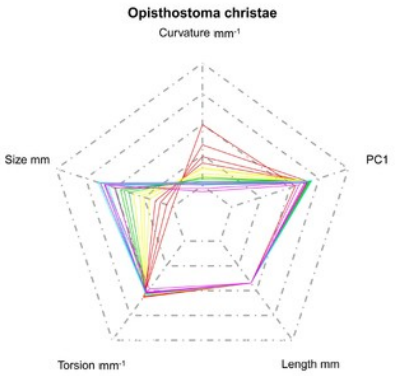

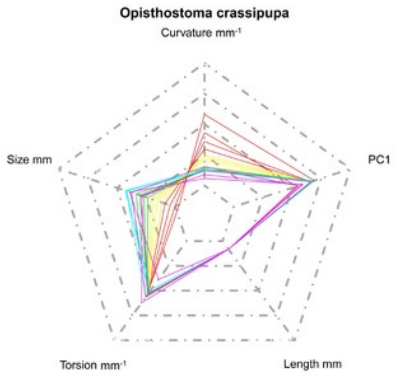

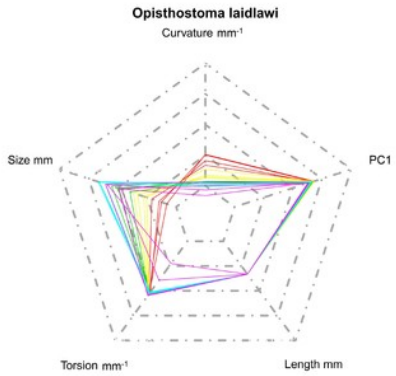

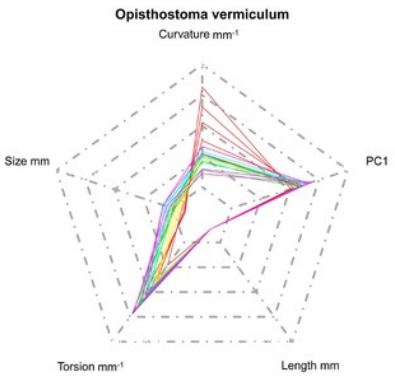

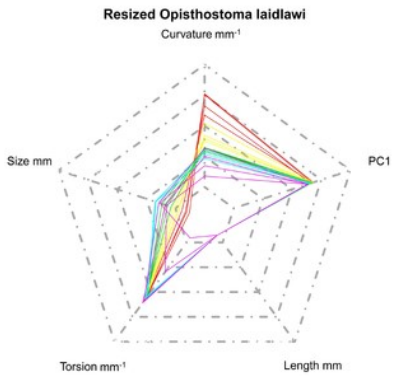

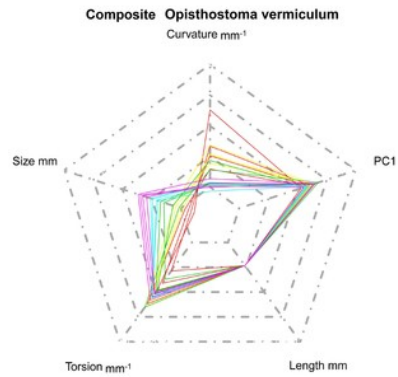

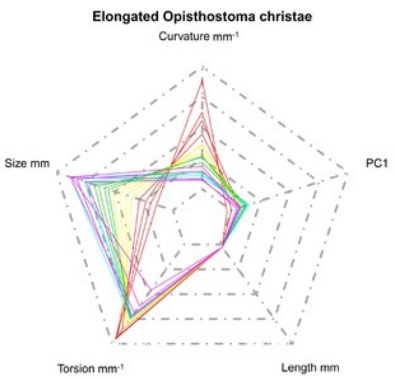

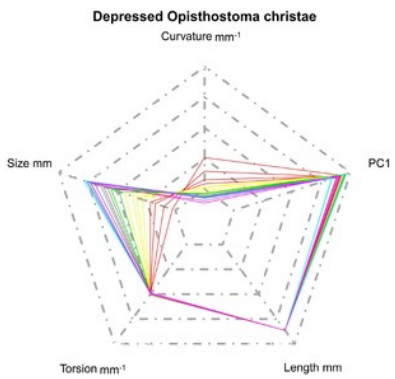

Figure 6

Dendrogram from permutation distribution clustering of the aperture ontogeny profiles of eight shells.

(A) Dendrogram from permutation distribution clustering of the four aperture ontogeny profiles, namely, curvature, torsion, aperture size, and aperture shape scores, of eight shells. (B) Four dendrograms from permutation distribution clustering of eight shells, which each for the four aperture ontogeny profiles, namely, curvature, torsion, aperture size, and aperture shape scores.

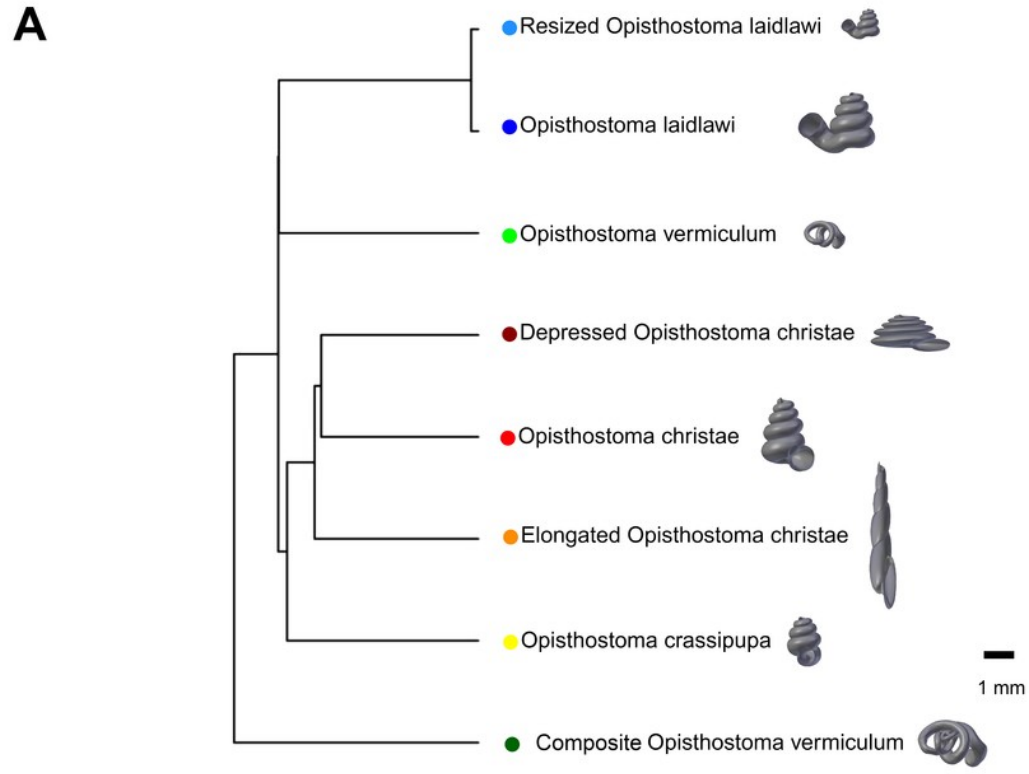

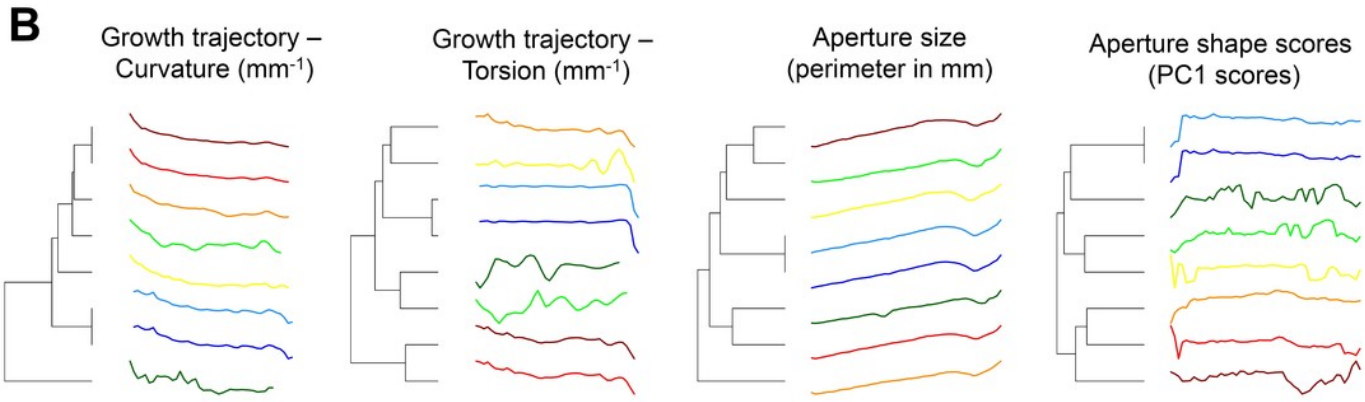

Figure 7

Non-metric multidimensional scaling (NMDS) 3D plots as shell morphospace.

The NMDS plots were generated from a dissimilarity matrix of eight *Opisthostoma* shells aperture ontogeny profiles, which were analysed by permutation distribution clustering.